UC San Diego
UC San Diego Previously Published Works

Title

Molecular organization of mammalian meiotic chromosome axis revealed by expansion STORM microscopy

Permalink

Journal

ISSN

Authors

Xu, Huizhong
Tong, Zhisong
Ye, Qing
et al.

Publication Date

DOI

Peer reviewed

Molecular organization of mammalian meiotic chromosome axis revealed by expansion STORM microscopy

Huizhong Xu[a,1], Zhisong Tong[a,1], Qing Ye[a,b,c,1], Tengqian Sun[a,1], Zhenmin Hong[a,1], Lunfeng Zhang[d], Alexandra Bortnick[e], Sunglim Cho[e], Paolo Beuzer[a], Joshua Axelrod[a], Qiongzheng Hu[a], Melissa Wang[a], Sylvia M. Evans[d], Cornelis Murre[e], Li-Fan Lu[e], Sha Sun[f], Kevin D. Corbett[g,h,i], and Hu Cang[a,2]

[a]Waitt Advanced Biophotonics Center, Salk Institute for Biological Studies, La Jolla, CA 92037; [b]The MOE Key Laboratory of Weak-Light Nonlinear Photonics, School of Physics and TEDA Applied Physics School, Nankai University, Tianjin 300071, China; [c]Interdisciplinary Research Center for Cell Responses, Nankai University, Tianjin 300071, China; [d]Skaggs School of Pharmacy and Pharmaceutical Sciences, University of California San Diego, La Jolla, CA 92093; [e]Division of Biological Sciences, University of California San Diego, La Jolla, CA 92093; [f]Department of Developmental and Cell Biology, University of California, Irvine, CA 92697; [g]Department of Cellular and Molecular Medicine, University of California San Diego, La Jolla, CA 92093; [h]Department of Chemistry, University of California San Diego, La Jolla, CA 92093; and [i]Ludwig Institute for Cancer Research, San Diego Branch, La Jolla, CA 92093

During prophase I of meiosis, chromosomes become organized as loop arrays around the proteinaceous chromosome axis. As homologous chromosomes physically pair and recombine, the chromosome axis is integrated into the tripartite synaptonemal complex (SC) as this structure's lateral elements (LEs). While the components of the mammalian chromosome axis/LE—including meiosis-specific cohesin complexes, the axial element proteins SYCP3 and SYCP2, and the HORMA domain proteins HORMAD1 and HORMAD2—are known, the molecular organization of these components within the axis is poorly understood. Here, using expansion microscopy coupled with 2-color stochastic optical reconstruction microscopy (STORM) imaging (ExSTORM), we address these issues in mouse spermatocytes at a resolution of 10 to 20 nm. Our data show that SYCP3 and the SYCP2 C terminus, which are known to form filaments in vitro, form a compact core around which cohesin complexes, HORMADs, and the N terminus of SYCP2 are arrayed. Overall, our study provides a detailed structural view of the meiotic chromosome axis, a key organizational and regulatory component of meiotic chromosomes.

synaptonemal complex | meiosis | chromosome axis | expansion microscopy | STORM

During prophase I of meiosis, homologous chromosomes recognize one another and become physically linked through the formation of the synaptonemal complex (SC), which bridges the axes of paired homologs, with each axis referred to as the lateral element (LE) (1). Chromosome axes play a central role in meiotic chromosome dynamics: The axis assembles in early meiotic prophase (leptotene/zygotene) and is required to initiate meiotic recombination and homolog recognition (2, 3). As homologs associate at sites of recombination, the axis is remodeled to suppress further recombination (4, 5) and becomes integrated into the assembling SC. The SC is fully assembled at pachytene and is then disassembled after recombination to allow further chromosome compaction and segregation in the meiosis I division.

Although axis/LE protein components have been identified in various model organisms, their physical organization remains poorly understood. In *Mus musculus*, the known axis protein components include the axial element proteins SYCP2 and SYCP3 (6, 7), the cohesin complexes (8), and HORMA domain proteins HORMAD1 and HORMAD2 (4). SYCP2 and SYCP3 bind one another through their coiled-coil C termini (9) and form filaments in vitro (10). SYCP2 also possesses a structured N-terminal domain with putative roles in chromatin localization (11) followed by a conserved "closure motif" that binds HORMAD proteins (10). HORMADs further possess closure motifs at their C termini, presumably allowing for head-to-tail oligomerization

of these proteins (10, 12). Major questions remain including how cohesin complexes are linked to the axis core, and how the axis is ultimately integrated into the tripartite SC.

With nanometer resolution, immunogold electron microscopy (EM) studies have suggested that the axis/LE might contain multilayered substructures (2, 13) in mammalian SC. However, as the labeling density of immunogold EM is low and multicolor EM is difficult, the construction of localization maps of different proteins with respect to one another in the chromosome axis remains challenging.

Recently, superresolution light microscopy methods, including stochastic optical reconstruction microscopy (STORM) (14), photoactivated localization microscopy (PALM) (15), structured illumination microscopy (SIM) (16), and expansion microscopy

Significance

The meiotic chromosome axis plays important roles in chromosome dynamics in mammalian meiosis, including in homologous chromosome pairing, synapsis, recombination, and segregation. Defects in chromosome axis structural integrity have been linked to various diseases, such as infertility, birth defects, and premature ovarian failure. Despite its importance, the molecular organization of the protein components within the chromosome axis remains poorly understood. Here, we address these questions by imaging the paired chromosome axes in mouse mid-prophase spermatocytes using expansion microscopy coupled with stochastic optical reconstruction microscopy (STORM), which provides 10- to 20-nm resolution for structural investigation. Our data reveal that the various axis proteins adopt a core-and-shell type organization, which provides a detailed view of meiotic chromosome axis organization at unprecedented resolution.
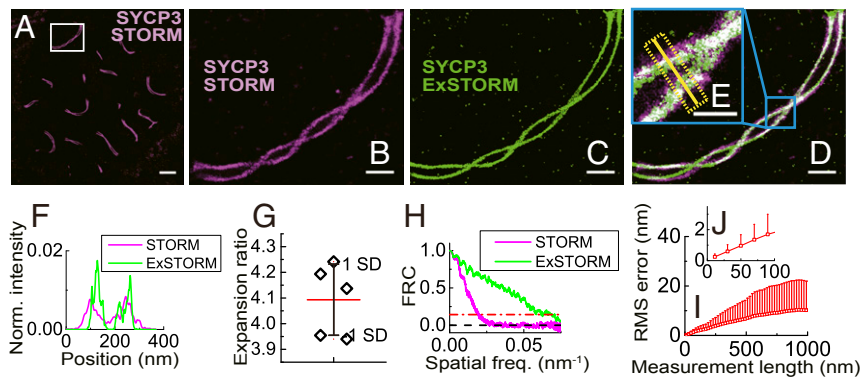
CELL BIOLOGY

Fig. 1. The ExSTORM procedure produced homogenously expanded samples for meiotic chromosome axis proteins, with improved resolution. (*A*) A STORM image (magenta) of a hypotonically spread mouse pachytene spermatocyte stained for SYCP3. (*B*) The magnified view of 1 meiotic chromosome within the boxed region in *A*. (*C*) ExSTORM image (green) of the same chromosome after expansion. (*D*) Overlay of (*B*) preexpansion image (magenta) and (*C*) post-expansion image (green). Overlapped signals are shown in white. (*E*) The magnified view of the blue boxed region in *D*. (*F*) Line profiles of SYCP3 intensity taken along the yellow line in *E*, with ExSTORM data showing sharper peak distributions than STORM data. (*G*) Expansion ratio values (diamonds) calculated by comparing preexpansion and postexpansion STORM images from 5 independent expansion samples, with mean value (red line) and SD (black bar) of 4.09 ± 0.14. (*H*) FRC measurement of resolution shows a 2D resolution of 52.2 nm for the STORM image (*B*) and 14.8 nm for the ExSTORM image (*C*). Similar FRC analysis on 5 independent expansion samples yields resolutions of 48.5 ± 7.3 nm (SD) for STORM and 17.9 ± 4.4 nm (SD) for ExSTORM. (*I*) Root-mean-square (RMS) length measurement error [mean (squares) + 1 SD (bars) for 5 independent expansion samples] in between preexpansion and postexpansion STORM images following the method in ref. 26. The measurement error is 10 nm at length scale of 1 μm, suggesting a distortion of 1%. (*J*) Zoom-in view of (*I*) at 0- to 100-nm length range. The measurement error is 0.96 nm at length scale of 50 nm, suggesting a distortion of 1.9%. (Scale bars: 2 μm in *A*; 500 nm in *B–D*; 200 nm in *E*.)

(17), have been used to probe the axis/LE substructure. Studies using CRISPR/Cas9-based epitope tagging with STORM/PALM imaging methods (18) in *Caenorhabditis elegans* showed that meiosis-specific HORMA domain proteins span a gap between cohesin complexes and the central region of the SC. Another study utilized expansion microscopy coupled with SIM to examine the 3D architecture of *Drosophila* SC, and revealed that C(2)M, a kleisin-like cohesin component, lies slightly above/below the layers of the transverse filament protein C(3)G (19). Both of the above studies suggest that the different axis proteins form layered structures with distinct locations for each protein. Compared to *C. elegans* and *Drosophila*, mammals usually contain additional axial element proteins SYCP2 and SYCP3 (20), whose deficiency leads to male sterility and female subfertility (6, 9, 21, 22). Thus, here we investigate the architecture of the mammalian meiotic chromosome axis with the major protein components including HORMADs, cohesin, SYCP2, and SYCP3.

Here, in order to study the organization of the axis/LE components in mice with high resolution, we modified recent expansion microscopy protocols (17, 23) to render them compatible with STORM (ExSTORM). Using this method, we enlarged *M. musculus* pachytene spermatocytes 4-fold and visualized chromosome axis/LE components by 2-color STORM imaging. This approach enabled 10 to 20 nm of 2D resolution for both colors, which is well suited to probe substructures in the 30- to 100-nm-wide meiotic chromosome axis. Our data suggest a core-shell–like arrangement for the various axis/LE proteins, with filaments of SYCP3 and the SYCP2 C terminus forming a core around which cohesin and HORMADs are arranged, potentially through linkage to the SYCP2 N terminus. These data show the potential for combining expansion and STORM microscopy to uncover detailed structural information on cellular substructures, and reveal the internal structure of the meiotic chromosome axis at unprecedented resolution.

Results

Principles and Resolution of ExSTORM.
For ExSTORM imaging on mouse meiotic chromosome structures, mouse pachytene spermatocytes (Fig. 1*A*), either hypotonically spread or in situ fixed, were immunostained with primary antibodies following standard immunofluorescence procedures. A hydrogel was then infused into the cells, with the primary antibodies cross-linked to the

hydrogel through a bifunctional cross-linker (acrylic acid *N*-hydroxysuccinimide ester) (23). After using proteinase K and micrococcal nuclease to dissociate the antibodies from the cellular antigens, the hydrogel was expanded by dialysis in a low ionic strength buffer. Dye-conjugated secondary antibodies against the primary antibodies were then used to stain the hydrogel.

We first validated that our experimental workflow of ExSTORM preserves the structural features of the pachytene chromosome axes at 50-nm length scales (Fig. 1*A*). As shown in Fig. 1 *B–D*, overlaying a preexpansion STORM image with a postexpansion ExSTORM image on the same chromosome shows good overlap, with the expansion ratio calculated as 4.09 ± 0.14 (mean $\pm$ SD from 5 samples) (Fig. 1*G*) in our STORM imaging buffer. Therefore, all distances recorded from expansion samples in this report are divided by this expansion ratio, so that they represent the original biological dimensions.

Consistent with prior findings using standard expansion microscopy (17), we find that regions where features are close to each other are better resolved after expansion, with the ExSTORM signal line profile showing narrower peak distributions than STORM (Fig. 1 *E* and *F*). As the typical *x*–*y* resolution for STORM is 40 to 50 nm (24), a 4-fold expansion of the sample would effectively give a resolution of 10 to 20 nm. Indeed, when we compared side-by-side the resolution of STORM and ExSTORM for imaging the same chromosomes labeled with SYCP3, we found that the preexpansion and postexpansion resolutions are 48.5 ± 7.3 and 17.9 ± 4.4 nm (mean $\pm$ SD), respectively, using Fourier ring correlation (FRC) (25) analysis, suggesting that ExSTORM provides a 3-fold resolution improvement compared to STORM (Fig. 1*H*).

We carefully measured the distortion introduced by hydrogel expansion using the distortion vector field method (26), and found that this distortion is 1.0% at a length scale of 1 μm and 1.9% at a length scale of 50 nm (Fig. 1 *I* and *J* and *SI Appendix*, Fig. S2), indicating that spatial expansion of the sample is mostly homogeneous. Immunostaining spread chromosomes with antibodies against SYCP2, HORMAD1, and cohesin also shows good preservation of structure after expansion (*SI Appendix*, Fig. S3).

Thus, ExSTORM is well suited to probe substructures in the meiotic chromosome axis, which is 30 to 100 nm wide. Moreover, 2-color imaging allows in situ comparison of localizations of
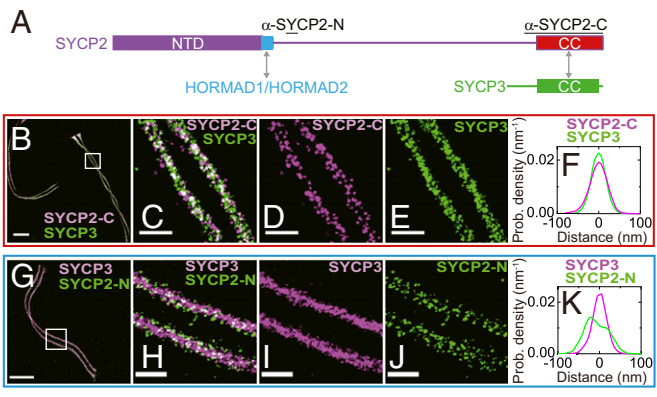
Fig. 2. Two-color ExSTORM images of spread chromosomes immunostained for SYCP2 and SYCP3. (*A*) Schematic of the *M. musculus* SYCP2 protein, with its N-terminal domain (NTD; residues 1 to 394), closure motif (blue), and C-terminal coiled-coil (CC) domain indicated. SYCP2 likely interacts with HORMADs and SYCP3 through its closure motif and CC domain, respectively. The immunogenic regions for the SYCP2-N and SYCP2-C antibodies are marked. (*B*) Two-color ExSTORM image on spread chromosomes labeled with SYCP3 and SYCP2 C terminus. (*C–E*) Zoom-in views of the boxed region shown in *B*, with SYCP2 C terminus showing a similar width to SYCP3, as analyzed by distance distributions (*F*) (from 3 cells, 4 chromosomes), with Gaussian fits in *SI Appendix*, Fig. S16*A*. (*G*) Two-color ExSTORM image on spread chromosomes labeled with SYCP3 and SYCP2 N terminus. (*H–J*) Zoom-in views of the boxed region shown in *G*, with SYCP2 N terminus showing broader width than that of SYCP3, as analyzed by distance distributions (*K*) (from 2 cells, 4 chromosomes), with Gaussian fits in *SI Appendix*, Fig. S16*B*. (Scale bars: 1 μm in *B* and *G*; 200 nm in *C–E* and *H–J*.)

different proteins within the LE with more confidence, despite the slight distortion introduced by local variations in expansion ratio. In our imaging setup, both colors have equivalent resolutions with no discernible misalignment (*SI Appendix*, Fig. S5). To further confirm that ExSTORM procedure preserves SC structure, we imaged the localizations of SYCP3 together with the SC transverse filament protein SYCP1 (*SI Appendix*, Fig. S6). Consistent with previous EM and STORM results (27, 28), the SYCP1 N terminus lies in the middle of the SC central region, 108.1 ± 3.4 nm (SD) away from the paired LEs labeled by SYCP3. The SYCP1 C terminus is located 25.5 ± 2.5 nm (SD) more interior than SYCP3.

Organization of SYCP3 and SYCP2 in the Chromosome Axis. We next performed 2-color ExSTORM imaging to determine the localization patterns of each axis/LE protein compared to SYCP3. We first examined SYCP2, a large protein (1,500 residues in *M. musculus*) known to oligomerize with SYCP3 through its coiled-coil C terminus in vitro (Fig. 2*A* and *SI Appendix*, Fig. S1) (9, 10). The N terminus of SYCP2 contains a 20-residue-long closure motif sequence, which shares homology to the C termini of HORMADs and was found to interact with HORMAD2. It also contains an ordered domain reported to interact with several chromatin-associated proteins (10), suggesting that this domain might serve the function of recruiting SYCP2 onto chromatin. In order to confirm these interactions in vivo, we first colabeled meiotic chromosomes with antibodies against SYCP3 and the C terminus of SYCP2 (Fig. 2 *B–F*). Indeed, we observed good colocalization between SYCP2-C and SYCP3. By analyzing the regions where the paired axes appear aligned in parallel (i.e., frontal view) (*SI Appendix*, Fig. S4), we determined that SYCP3 and SYCP2-C show similar distribution widths of 48.0 ± 8.1 nm (SD) and 40.6 ± 5.4 nm (SD), respectively.

The SYCP2 N terminus contains an ordered domain and a HORMAD-binding closure motif, followed by a ~800-residue stretch of disordered sequence (Fig. 2*A* and *SI Appendix*, Fig. S1). To determine the arrangement of SYCP2 N terminus in the

axis, we costained meiotic chromosomes with antibodies (*SI Appendix*, Fig. S1) targeting SYCP3 and the SYCP2 N terminus near its closure motif. Our ExSTORM data (Fig. 2 *G–K*) revealed that the SYCP2 N terminus [width, 84.8 ± 8.9 nm (SD)] is more broadly distributed than SYCP3 [width, 39.1 ± 3.8 nm (SD)]. Consistently, in an independent 2-color experiment in which we directly compared the localization of the SYCP2 N and C termini, by costaining both termini of SYCP2 with their respective antibodies, we also found that SYCP2-N exhibits a broader distribution width than SYCP2-C (*SI Appendix*, Fig. S7). These data support a model in which the coiled-coil filaments of SYCP3 and the SYCP2 C terminus form an axis core, around which the SYCP2 N termini are arrayed, and SYCP2-N may serve to link other proteins or chromatin to the SYCP3/SYCP2-C core.

Organization of Meiotic HORMADs in the Chromosome Axis. We next examined the organizations of HORMAD1 and HORMAD2, which are known to localize to the chromosome axis (4) and are required both for wild-type levels of meiotic DNA double-strand breaks (DSBs) and for proper homolog-directed repair of these DSBs (29). Previous in vitro studies have identified closure motifs in both the SYCP2 N-terminal region and the HORMAD C termini, which likely mediate HORMAD recruitment and head-to-tail oligomerization, respectively (10, 30) (Fig. 2*A* and *SI Appendix*, Fig. S1). In order to examine the localization of HORMADs within the chromosome axis, we colabeled meiotic chromosomes with SYCP3 and either HORMAD1 or HORMAD2, and imaged them using ExSTORM (Fig. 3). Similar to our findings with the SYCP2 N terminus, frontal views of the chromosome axes revealed that HORMAD1 adopts a wider distribution than SYCP3 (Fig. 3 *A–C*). Histogram analysis further showed that, while SYCP3 shows 1 peak, HORMAD1 exhibits as 2 peaks bracketing the SYCP3 peak (Fig. 3*D* and *SI Appendix*, Fig. S16*D*). The total width of HORMAD1 distribution is 76.9 ± 5.1 nm (SD), larger than the width of SYCP3 [30.0 ± 2.2 nm (SD)]. These data suggest HORMAD1 mostly coats the outside of the SYCP3 core. We then imaged the axial views of the chromosome axis/LE stained for SYCP3 and HORMAD1 (Fig. 3 *E–G* and *SI Appendix*, Figs. S9 and S10), and found HORMAD1 is also distributed more broadly than SYCP3, with reduced signal in the SYCP3 core, confirming that SYCP3 and HORMAD1 appear to form a core-shell–like structure. Notably, a conventional STORM image (*SI Appendix*, Fig. S8) on HORMAD1 and SYCP3 stained axis only shows bigger width of HORMAD1 but cannot reveal the core-shell–like structure.
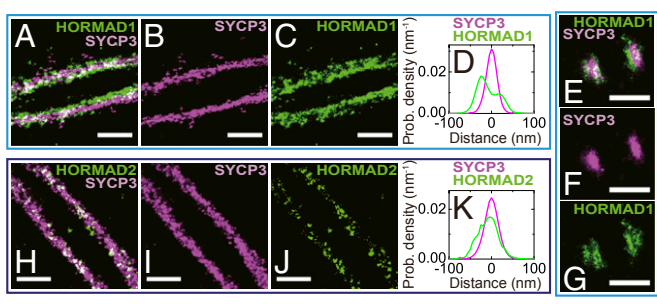

Fig. 3. Two-color ExSTORM images of spread chromosomes immunostained for meiotic HORMADs. (*A–C*) ExSTORM image on a pachytene chromosome labeled with SYCP3 and HORMAD1. (*D*) Distance distributions (from 4 cells, 6 chromosomes) showing that HORMAD1 has broader width than SYCP3, with Gaussian fits in *SI Appendix*, Fig. S16*D*. (*E–G*) An axial ExSTORM image on a pachytene chromosome labeled with SYCP3 and HORMAD1, showing most HORMAD1 signals are outside the SYCP3 core. (*H–J*) ExSTORM image on a pachytene chromosome labeled with SYCP3 and HORMAD2. (*K*) Distance distributions (from 3 cells, 5 chromosomes) showing that HORMAD2 spans wider than SYCP3, with Gaussian fits in *SI Appendix*, Fig. S16*E*. (Scale bars: 200 nm.)
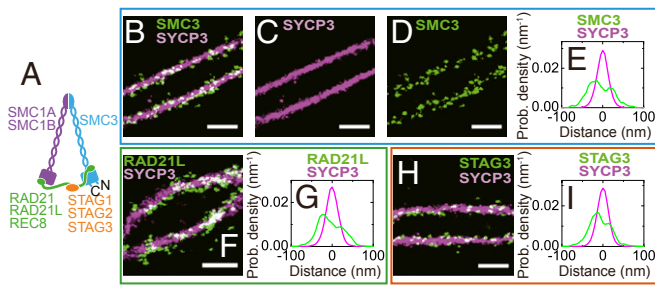
Fig. 4. Two-color ExSTORM images of spread chromosomes immunostained for cohesin subunits. (*A*) Schematic of a meiotic cohesin complex containing 4 subunits: 2 SMCs (purple and cyan), 1 kleisin (green), and 1 stromal antigen protein (orange oval). (*B–D*) ExSTORM image of a meiotic chromosome labeled with SMC3 C terminus and SYCP3, with SMC3 showing broader width along LE than that of SYCP3, as analyzed by distance distributions (from 4 cells, 5 chromosomes) in *E*, with Gaussian fits in *SI Appendix*, Fig. S16*H*. (*F*) ExSTORM image of a meiotic chromosome labeled with RAD21L and SYCP3, with distance distributions (from 4 cells, 4 chromosomes) shown in *G*, and Gaussian fits in *SI Appendix*, Fig. S16*I*. (*H*) ExSTORM image of a meiotic chromosome labeled with STAG3 and SYCP3, with distance distributions (from 3 cells, 6 chromosomes) shown in *I*, and Gaussian fits in *SI Appendix*, Fig. S16*J*. (Scale bars: 200 nm.)

We then imaged HORMAD2 localization in the chromosome axis/LE. While HORMAD2 is less abundant than HORMAD1 (Fig. 3 *H–J*), it nevertheless also exhibits a wider distribution [width, 72.4 ± 13.1 nm (SD)] than SYCP3 [width, 38.5 ± 5.3 nm (SD)] (Fig. 3*K*).

Next, we examined localizations of HORMADs at other prophase substages. As shown in *SI Appendix*, Fig. S11, at early zygotene stage, where the SYCP3 filaments are unpaired, HORMADs [width, 91.5 ± 6.7 nm (SD)] also coat the outside of the SYCP3 core [width, 35.0 ± 5.1 nm (SD)]; at diplotene stage, when paired axes undergo desynapsis, HORMADs [width, 106.6 ± 3.3 nm (SD)] also exhibit a broader width than SYCP3 [width, 82.3 ± 2.6 nm (SD)]. Overall, our ExSTORM data suggest that the core-shell–like organization between SYCP3 and HORMADs is retained throughout chromosome axis assembly, integration into the SC, and disassembly during meiotic prophase I.

Organization of Cohesin Complexes in the Chromosome Axis. The meiotic cohesin complexes consist of 2 structural maintenance of chromosomes proteins (SMC1A/SMC1B and SMC3), an α-kleisin protein (RAD21, RAD21L, or REC8), and a stromal antigen protein (STAG1, STAG2, or STAG3) (31) (Fig. 4*A*). Knockout of the cohesin subunits SMC1B, RAD21L, REC8, or STAG3 in mice leads to defective synapsis of homologous chromosomes in prophase I, affects the overall length of the axis, and causes sterility (32–36). We wondered whether ExSTORM might illuminate how cohesin complexes are organized within the axes (Fig. 4 and *SI Appendix*, Fig. S12). We first stained meiotic chromosomes with antibodies against the SMC3 C terminus head domain, near the primary DNA binding site of the complex (37, 38), along with SYCP3 (Fig. 4 *B–E*). We found that most SMC3-C signals are located near the boundary of the SYCP3 core, with SMC3-C distribution showing 2 peaks [total width, 85.7 ± 5.3 nm (SD)] bracketing the SYCP3 peak [width, 32.4 ± 4.3 nm (SD)], similar to the distribution pattern of HORMAD1. Consistently, an independent 2-color experiment on SMC3 and HORMAD1 stained chromosomes shows similar distribution widths for both proteins (*SI Appendix*, Fig. S14).

We next examined the localizations of other cohesin subunits. Biochemical and structural analyses have shown that the N and C termini of SMC1 and SMC3 head domains interact with kleisin and stromal antigen subunits (39, 40). Consistent with this, our ExSTORM imaging on meiotic chromosomes with antibodies

against RAD21L and STAG3 shows both proteins have similar distribution patterns to that of the SMC3 C terminus, with widths of 87.7 ± 14.2 nm (SD) and 71.3 ± 10.9 nm (SD), respectively (Fig. 4 *F–I*). Such a core-shell–like structure between cohesin and SYCP3 cannot be resolved by our conventional STORM imaging (*SI Appendix*, Fig. S13).

Having examined the localizations of all major axis proteins above, we further confirmed that their localization patterns are not an artifact due to hypotonic spreading, by imaging in situ fixed whole cells (*SI Appendix*, Fig. S15). Despite lower antibody binding efficiency in directly fixed cells, the measured distribution widths for SYCP3 [38.9 ± 3.9 nm (SD)], SYCP2-N [66.9 ± 3.0 nm (SD)], HORMAD1 [90.8 ± 13.9 nm (SD)], and SMC3-C [73.3 ± 8.2 nm (SD)] were consistent with our hypotonic spreading results.

Discussion

Here, we show that the combination of expansion microscopy with STORM (ExSTORM) is a robust method that provides a 2D spatial resolution of 10 to 20 nm. Since its invention (17), expansion microscopy has been developing at fast pace. Higher expansion ratios up to 10- to 20-fold have been achieved by using different gel recipes (41) or multiple rounds of expansion (42). Combinations of expansion microscopy with other superresolution microscopes, such as SIM (ExSIM) (19, 43), STED (ExSTED) (44–46), and lattice light sheet microscopy (ExLLSM) (47) have also been reported to boost the resolution and throughput of imaging. Meanwhile, with expansion ratio of 3 to 5, the homogeneity of expansion has been confirmed by imaging DNA origami nanorulers (48) and nuclear pore complexes (49). Here, by integrating expansion microscopy with STORM, we also confirm that our sample expansion is mostly homogeneous at 50 nm length scales. We use a series of 2-color ExSTORM experiments to reveal structural details of the meiotic chromosome axis/SC lateral element in mouse pachytene spermatocytes. Our data suggest that the axis/LE proteins appear to have a core-shell–like organization (Fig. 5) that has significant implications for meiotic chromosome architecture and function.

Our imaging suggests that the meiotic chromosome axial element proteins SYCP2 and SYCP3 form a compact 30- to 50-nm-wide axis core, which supports prior in vitro findings that their C-terminal coiled-coil regions can oligomerize into filaments. High-resolution structural information on SYCP2:SYCP3 coiled-coil tetramers has shown that each filament is 2 to 3 nm in width (10, 50), suggesting that the fully assembled axis comprises a bundle of such filaments. The SYCP2 N terminus, linked to the C-terminal coiled-coil region by an ~800-residue disordered region, is arranged
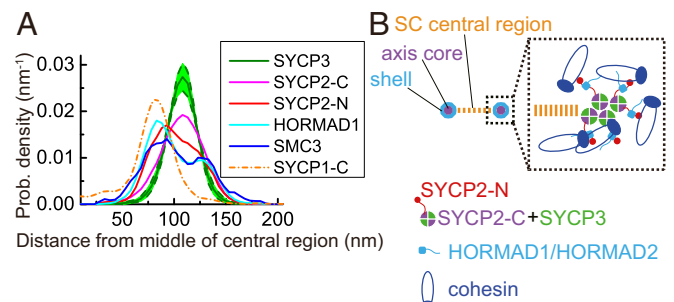

Fig. 5. Model of meiotic chromosome axis organizations in mouse pachytene chromosomes. (*A*) Overlay of the localization distributions of the major LE/axis components, determined from their 2-color experiments with respect to SYCP3. The ±1 SD boundaries for the SYCP3 distribution curves over these experiments are shown as dashed lines. The distance coordinate is plotted with respect to the N terminus of SYCP1, i.e., the middle of SC central region. (*B*) Model of the protein organizations in synapsed meiotic chromosome axes in the axial view.

as a "shell" around the compact axis core. This region of SYCP2 contains an ordered domain with putative roles in chromatin localization (11), and a HORMAD-interacting closure motif (10). Consistent with the identified direct interaction between SYCP2 and HORMAD2 (10), we find that the distribution widths of HORMAD1 [76.9 ± 5.1 nm (SD)], HORMAD2 [72.4 ± 13.1 nm (SD)], and the SYCP2 N terminus [84.8 ± 8.9 nm (SD)] are similar and significantly greater than that of SYCP3 [35.8 ± 5.4 nm (SD)] (*SI Appendix*, Table S2).

By investigating multiple epitopes on cohesin complexes, our data also shed light on the spatial localizations of cohesins in the chromosome axis. The SMC head, kleisin, and stromal antigen all exhibit broader distributions than SYCP3, suggesting cohesin complexes are located around the axis core and might associate with a component of the axis. While direct interactions between cohesin complexes and other axis components have not been identified in mammals, the SYCP2 ortholog Red1 in *Saccharomyces cerevisiae* has been demonstrated to closely associate with cohesin complexes (51). Thus, we speculate that cohesin complexes may associate directly or indirectly with SYCP2 to mediate anchoring of chromatin loops at the axis. Further work will be needed to identify and characterize this potential interaction.

Overall, our data demonstrate the utility of ExSTORM as an accessible imaging method that provides a ~3-fold resolution improvement over conventional STORM microscopy without significant additional instrumentation cost. Our use of ExSTORM to reveal previously unknown structural features of the meiotic chromosome axis/SC lateral element further illustrates the utility of the method as a bridge between conventional light microscopy and high-resolution structural methods including X-ray crystallography and cryo-EM.

Materials and Methods

More details of materials and methods can be found in *SI Appendix*. The usage of mice was approved by the Institutional Animal Care and Use Committees of Salk Institute, University of California San Diego, and University of California, Irvine.

Murine Spermatocyte Cell Spread Preparation. For cell spreading, we dissected testes from 2 35 days postpartum (dpp) and 2 41 dpp wild-type mice and followed the protocol described by de Boer et al. (52).

Immunostaining. The cell samples prepared above were blocked with 1% BSA and 0.1% Triton X-100 in PBS for 1 h. Samples were incubated with primary antibody at a concentration of 20 μg/mL in the blocking buffer at room temperature for 24 h, followed by incubation in 0.33 mM acrylic acid *N*-hydroxysuccinimide ester in PBS at room temperature for 2.5 h, before proceeding with the sample gelation and expansion protocols below.

Gelation, Digestion, and Postdigestion Staining. The immunostained samples were gelled in our monomer solution (*SI Appendix*) plus 0.2% (wt/wt) tetramethylethylenediamine and 0.2% (wt/wt) ammonium persulfate for 3 h at 37 °C. The polymerized gel was then immersed in 4 mL of 0.2 mg/mL proteinase K (Roche) in digestion buffer (*SI Appendix*) and incubated at 37 °C for 5 h. The gel was then incubated with 5 gel units/uL micrococcal nuclease (NEB) at 37 °C for 3 h. Digested gels were next placed in excess volumes of PBS for 2 h. The gels were then stained with Alexa 647- and CF568-conjugated secondary antibodies at room temperature overnight, followed by washing in 10 mM Tris, pH 8.0 buffer. The expanded hydrogels were then attached onto poly-L-lysine–coated cover glass for STORM imaging.

ExSTORM Imaging. STORM imaging of expanded samples was carried out on a Nikon Ti inverted microscope equipped with a 60× TIRF objective lens (N.A., 1.49). An ASI CRISP autofocus system (ASI Imaging) coupled with a 3D piezo stage (Physik Instruments) was used to lock in the focus during imaging. A 639-nm laser (Coherent Genesis; 1 W) and a 561-nm laser (MPB Communications; 2 W) were used, followed by activation with 405-nm laser (Coherent OBIS). A homemade dual-viewer was placed in front of an EMCCD (Andor iXon3) for 2-color imaging. Single-molecule blinking events were collected from a field of view (FOV) of 35 × 35 μm with an integration time of 50 ms for a total of about 150,000 frames. Alignment of the 2 colors in the FOV was determined using fluorescent beads. STORM images were analyzed by ThunderSTORM and MatlabSTORM (Github). Lateral drift was corrected by cross-correlations. The final images used in the figures were plotted by rendering each localization as a 2D Gaussian peak.

Image Analysis. We first manually fitted the central lines of the paired LEs/axes in each meiotic chromosome with fifth-order polynomial functions. We next calculated the protein distribution (with bin size of 5 nm) around LE by measuring the distance between their localizations to the fitted central lines. We rejected individual signals with distances larger than 80 nm for LE proteins from the central lines to avoid false or background signals that did not belong to the LE. Detailed analysis workflow is illustrated in *SI Appendix*, Fig. S4. The distributions of protein localizations were fitted by a single Gaussian or 2 Gaussians, depending on the shape of the distribution. The widths of the distributions were then determined as either the full width at half-maximum of a single Gaussian or the distance from the leftmost Gaussian's half-maximum position to the rightmost Gaussian's half-maximum position (*SI Appendix*, Fig. S16). The distribution widths and their SDs over the number of imaged chromosomes are tabulated in *SI Appendix*, Table S2.

Data Availability. All ExSTORM/STORM localization data used in this paper are available at the Open Science Framework (OSF) data repository (https://osf.io/mnh8r/).

1. D. Zickler, N. Kleckner, Meiotic chromosomes: Integrating structure and function. *Annu. Rev. Genet.* **33**, 603–754 (1999).
2. K. Ishiguro et al., Meiosis-specific cohesin mediates homolog recognition in mouse spermatocytes. *Genes Dev.* **28**, 594–607 (2014).
3. F. Baudat, Y. Imai, B. de Massy, Meiotic recombination in mammals: Localization and regulation. *Nat. Rev. Genet.* **14**, 794–806 (2013).
4. L. Wojtasz et al., Mouse HORMAD1 and HORMAD2, two conserved meiotic chromosomal proteins, are depleted from synapsed chromosome axes with the help of TRIP13 AAA-ATPase. *PLoS Genet.* **5**, e1000702 (2009).
5. I. Roig et al., Mouse TRIP13/PCH2 is required for recombination and normal higher-order chromosome structure during meiosis. *PLoS Genet.* **6**, e1001062 (2010).
6. L. Yuan et al., The murine SCP3 gene is required for synaptonemal complex assembly, chromosome synapsis, and male fertility. *Mol. Cell* **5**, 73–83 (2000).
7. H. H. Offenberg et al., SCP2: A major protein component of the axial elements of synaptonemal complexes of the rat. *Nucleic Acids Res.* **26**, 2572–2579 (1998).
8. I. Onn, J. M. Heidinger-Pauli, V. Guacci, E. Unal, D. E. Koshland, Sister chromatid cohesion: A simple concept with a complex reality. *Annu. Rev. Cell Dev. Biol.* **24**, 105–129 (2008).
9. F. Yang et al., Mouse SYCP2 is required for synaptonemal complex assembly and chromosomal synapsis during male meiosis. *J. Cell Biol.* **173**, 497–507 (2006).
10. A. M. V. West et al., A conserved filamentous assembly underlies the structure of the meiotic chromosome axis. *eLife* **8**, e40372 (2019).
11. J. Feng et al., Synaptonemal complex protein 2 (SYCP2) mediates the association of the centromere with the synaptonemal complex. *Protein Cell* **8**, 538–543 (2017).
12. A. M. V. West, E. A. Komives, K. D. Corbett, Conformational dynamics of the Hop1 HORMA domain reveal a common mechanism with the spindle checkpoint protein Mad2. *Nucleic Acids Res.* **46**, 279–292 (2018).
13. R. Ortiz, A. Kouznetsova, O. M. Echeverría-Martínez, G. H. Vázquez-Nin, A. Hernández-Hernández, The width of the lateral element of the synaptonemal complex is determined by a multilayered organization of its components. *Exp. Cell Res.* **344**, 22–29 (2016).
14. M. J. Rust, M. Bates, X. Zhuang, Sub-diffraction-limit imaging by stochastic optical reconstruction microscopy (STORM). *Nat. Methods* **3**, 793–795 (2006).
15. E. Betzig et al., Imaging intracellular fluorescent proteins at nanometer resolution. *Science* **313**, 1642–1645 (2006).
16. M. G. Gustafsson, Surpassing the lateral resolution limit by a factor of two using structured illumination microscopy. *J. Microsc.* **198**, 82–87 (2000).
17. F. Chen, P. W. Tillberg, E. S. Boyden, Optical imaging. expansion microscopy. *Science* **347**, 543–548 (2015).
18. S. Köhler, M. Wojcik, K. Xu, A. F. Dernburg, Superresolution microscopy reveals the three-dimensional organization of meiotic chromosome axes in intact *Caenorhabditis elegans* tissue. *Proc. Natl. Acad. Sci. U.S.A.* **114**, E4734–E4743 (2017).
19. C. K. Cahoon et al., Superresolution expansion microscopy reveals the three-dimensional organization of the *Drosophila* synaptonemal complex. *Proc. Natl. Acad. Sci. U.S.A.* **114**, E6857–E6866 (2017).

CELL BIOLOGY

20. C. K. Cahoon, R. S. Hawley, Regulating the construction and demolition of the synaptonemal complex. *Nat. Struct. Mol. Biol.* **23**, 369–377 (2016).
21. L. Yuan *et al.*, Female germ cell aneuploidy and embryo death in mice lacking the meiosis-specific protein SCP3. *Science* **296**, 1115–1118 (2002).
22. B. Liebe, M. Alsheimer, C. Höög, R. Benavente, H. Scherthan, Telomere attachment, meiotic chromosome condensation, pairing, and bouquet stage duration are modified in spermatocytes lacking axial elements. *Mol. Biol. Cell* **15**, 827–837 (2004).
23. P. W. Tillberg *et al.*, Protein-retention expansion microscopy of cells and tissues labeled using standard fluorescent proteins and antibodies. *Nat. Biotechnol.* **34**, 987–992 (2016).
24. K. Prakash *et al.*, Superresolution imaging reveals structurally distinct periodic patterns of chromatin along pachytene chromosomes. *Proc. Natl. Acad. Sci. U.S.A.* **112**, 14635–14640 (2015).
25. R. P. Nieuwenhuizen *et al.*, Measuring image resolution in optical nanoscopy. *Nat. Methods* **10**, 557–562 (2013).
26. T. J. Chozinski *et al.*, Expansion microscopy with conventional antibodies and fluorescent proteins. *Nat. Methods* **13**, 485–488 (2016).
27. K. Schmekel *et al.*, Organization of SCP1 protein molecules within synaptonemal complexes of the rat. *Exp. Cell Res.* **226**, 20–30 (1996).
28. K. Schücker, T. Holm, C. Franke, M. Sauer, R. Benavente, Elucidation of synaptonemal complex organization by super-resolution imaging with isotropic resolution. *Proc. Natl. Acad. Sci. U.S.A.* **112**, 2029–2033 (2015).
29. Y. H. Shin *et al.*, Hormad1 mutation disrupts synaptonemal complex formation, recombination, and chromosome segregation in mammalian meiosis. *PLoS Genet.* **6**, e1001190 (2010).
30. Y. Kim *et al.*, The chromosome axis controls meiotic events through a hierarchical assembly of HORMA domain proteins. *Dev. Cell* **31**, 487–502 (2014).
31. A. Ward, J. Hopkins, M. Mckay, S. Murray, P. W. Jordan, Genetic interactions between the meiosis-specific cohesin components, STAG3, REC8, and RAD21L. *G3 (Bethesda)* **6**, 1713–1724 (2016).
32. C. A. Hodges, E. Revenkova, R. Jessberger, T. J. Hassold, P. A. Hunt, SMC1beta-deficient female mice provide evidence that cohesins are a missing link in age-related nondisjunction. *Nat. Genet.* **37**, 1351–1355 (2005).
33. E. Revenkova *et al.*, Cohesin SMC1 beta is required for meiotic chromosome dynamics, sister chromatid cohesion and DNA recombination. *Nat. Cell Biol.* **6**, 555–562 (2004).
34. Y. Herrán *et al.*, The cohesin subunit RAD21L functions in meiotic synapsis and exhibits sexual dimorphism in fertility. *EMBO J.* **30**, 3091–3105 (2011).
35. H. Xu, M. D. Beasley, W. D. Warren, G. T. van der Horst, M. J. McKay, Absence of mouse REC8 cohesin promotes synapsis of sister chromatids in meiosis. *Dev. Cell* **8**, 949–961 (2005).
36. J. Hopkins *et al.*, Meiosis-specific cohesin component, Stag3 is essential for maintaining centromere chromatid cohesion, and required for DNA repair and synapsis between homologous chromosomes. *PLoS Genet.* **10**, e1004413 (2014).
37. F. U. Seifert, K. Lammens, G. Stoehr, B. Kessler, K. P. Hopfner, Structural mechanism of ATP-dependent DNA binding and DNA end bridging by eukaryotic Rad50. *EMBO J.* **35**, 759–772 (2016).
38. Y. Li *et al.*, Structural basis for Scc3-dependent cohesin recruitment to chromatin. *eLife* **7**, e38356 (2018).
39. K. Hara *et al.*, Structure of cohesin subcomplex pinpoints direct shugoshin-Wapl antagonism in centromeric cohesion. *Nat. Struct. Mol. Biol.* **21**, 864–870 (2014).
40. T. G. Gligoris *et al.*, Closing the cohesin ring: Structure and function of its Smc3-kleisin interface. *Science* **346**, 963–967 (2014).
41. S. Truckenbrodt *et al.*, X10 expansion microscopy enables 25-nm resolution on conventional microscopes. *EMBO Rep.* **19**, e45836 (2018).
42. J. B. Chang *et al.*, Iterative expansion microscopy. *Nat. Methods* **14**, 593–599 (2017).
43. A. R. Halpern, G. C. M. Alas, T. J. Chozinski, A. R. Paredez, J. C. Vaughan, Hybrid structured illumination expansion microscopy reveals microbial cytoskeleton organization. *ACS Nano* **11**, 12677–12686 (2017).
44. D. Unnersjö-Jess *et al.*, Confocal super-resolution imaging of the glomerular filtration barrier enabled by tissue expansion. *Kidney Int.* **93**, 1008–1013 (2018).
45. M. Gao *et al.*, Expansion stimulated emission depletion microscopy (ExSTED). *ACS Nano* **12**, 4178–4185 (2018).
46. D. Gambarotto *et al.*, Imaging cellular ultrastructures using expansion microscopy (U-ExM). *Nat. Methods* **16**, 71–74 (2019).
47. R. Gao *et al.*, Cortical column and whole-brain imaging with molecular contrast and nanoscale resolution. *Science* **363**, eaau8302 (2019).
48. M. B. Scheible, P. Tinnefeld, Quantifying expansion microscopy with DNA origami expansion nanorulers. bioRxiv:10.1101/265405 (14 February 2018).
49. L. Pesce, M. Cozzolino, L. Lanzanò, A. Diaspro, P. Bianchini, Measuring expansion from macro- to nanoscale using NPC as intrinsic reporter. *J. Biophotonics* 10.1002/jbio.201900018 (2019).
50. J. L. Syrjänen, L. Pellegrini, O. R. Davies, A molecular model for the role of SYCP3 in meiotic chromosome organisation. *eLife* **3**, e02963 (2014).
51. X. Sun *et al.*, Transcription dynamically patterns the meiotic chromosome-axis interface. *eLife* **4**, e07424 (2015).
52. E. de Boer, F. G. Lhuissier, C. Heyting, Cytological analysis of interference in mouse meiosis. *Methods Mol. Biol.* **558**, 355–382 (2009).